THE UNIVERSITY of EDINBURGH

Edinburgh Research Explorer

Generation of Mechanical Frequency Related Harmonics in the Stray Flux Spectra of Induction Motors Suffering from Rotor Electrical Faults

OPEN ACCESS

Generation of Mechanical Frequency Related Harmonics in the Stray Flux Spectra of Induction Motors Suffering from Rotor Electrical Faults

Konstantinos N. Gyftakis, *Senior Member, IEEE*, Panagiotis A. Panagiotou and Sang Bin Lee, *Fellow, IEEE*,

Abstract — Lately, the monitoring and analysis of the induction motor stray flux has been a modern trend and significant research work was accomplished. Most papers have focused on the monitoring of rotor electrical faults around the fundamental stray flux signature, imitating in this way the traditional Motor Current Signature Analysis (MCSA). However, such signatures may still have some disadvantages leading to false alarms. This is the motivation behind the use of alternative signatures such as, in this particular case, the mechanical frequency. The existence of the mechanical frequency in the stator current is still the best signature for detection of the mixed rotor eccentricity fault and load imbalances. Even healthy motors present this harmonic due to some low-level inherent eccentricity and inherent load oscillations. Despite that, it will be shown for the first time in this paper that the mechanical frequency associated harmonics in the stray flux is possible to originate purely from rotor electrical faults. Those signatures present significant sensitivity to the broken bar fault severity. Moreover, they are advantageous for low load operation compared to traditional signatures. Finally, the sidebands of the mechanical frequency related harmonics are very sensitive to the broken rotor bar fault while quite immune to the number of the rotor bars.

Index Terms — Fault diagnosis, Flux Monitoring, Induction motors, Rotor Faults.

I. INTRODUCTION

ALTHOUGH induction motors are robust devices, faults may appear and either directly or progressively, will lead to degradation and eventual motor failure. An unexpected motor failure leads to increased financial losses not only from the transportation, maintenance, service and repair of the motor but most importantly from the interruption of the production process.

K. N. Gyftakis is with the School of Engineering and the Institute for Energy Systems, The University of Edinburgh, UK (e-mail: k.n.gyftakis@ieee.org).

P. A. Panagiotou is with the Research Institute for Future Transport and Cities, Coventry University, CV12JH, UK (e-mail: panagio4@uni.coventry.ac.uk)

S. B. Lee is with Department of Electrical Engineering, Korea University, Seoul, 02841 Korea (e-mail: sangbinlee@korea.ac.kr).

This is the main motivation behind the rapid advance in the area of electrical machines condition monitoring and fault diagnosis worldwide.

Many different methods have been proposed for reliable fault detection in induction machines [1]-[4]. Those methods differ on the diagnostic variable to be used for health information extraction and the signal analysis and processing. The stator current [5], electric power [6] and torque [7] are some of the most widely used signals. Depending on the operating state of the motor (steady state or transient), different signal processing techniques include the family of Park's Vector Approach techniques [8]-[9], Fast Fourier Transform (FFT) [10], Short Time Fourier Transform (STFT) [11]-[12], Wavelets [13]-[14], Hilbert [15] and MUSIC [16]. Recently, significant attention has been given to advancement of the monitoring and analysis of the stray flux.

The reasons behind the latest flux-monitoring trend are many. Firstly, depending on the flux direction (radial, axial or mix of both) different diagnostic information can be retrieved [17]-[18]. Moreover, the monitoring of the air-gap flux has proved a reliable diagnostic technique, although intrusive [19]-[20]. Furthermore, the flux spectral information is similar to that of the stator current, which means that there is a strong past expertise [21]. Moreover, multiple rotor faults happening at pole pitch-dependent locations tend to mask their existence in the stator current while cancelling out each other's asymmetry. In that sense, the stray flux monitoring is immune to faults with polar symmetry, and superior to the stator current. The term stray flux corresponds to magnetic flux lines radiating to the exterior of the machine's main magnetic circuit. This inherent weakness of the MCSA originates in the fact that the stator winding forms the stator magnetic field poles. Finally, the flux proves to be immune to certain phenomena, where the MCSA was leading to false diagnostic alarms [22].

In this paper, the authors are studying the associated to the mechanical frequency sidebands in the stray flux spectra under healthy and faulty induction motor operating conditions [23]. Extensive Finite Element Analysis (FEA) simulations and experimental testing with induction motors of different sizes, geometrical features and operating conditions has been carried out. The results show that, the

mechanical frequency related components in the stray flux are a strong indication of rotor electrical faults. So far, such harmonics have been associated with the mixed eccentricity fault, especially through the application of the MCSA. Moreover, the existence of such harmonics in the stator current of a healthy induction motor are known to be due to an inherent level of mixed eccentricity, typically below 10%. It will be shown that, the existence of such harmonics in the stray flux is due to inherent cage manufacturing asymmetries distorting the rotor field symmetry, such as porosity, magnetic anisotropy as well as actual faults such as broken rotor bars.

II. FINITE ELEMENT ANALYSIS

In this section, three induction motors are simulated with FEA under steady state operation. The characteristics of the three motors are shown in the following Table I. The investigation aims to study the impact of the motor size as well as the rotor slot number on the mechanical speed frequency in the radial flux spectra. All motors have been simulated under healthy operation, as well as with one broken rotor bar. Furthermore, Motor C is simulated under different broken rotor bar fault severity levels to allow for a close and detailed inspection of the severity impact on the frequency area under interest. A sensing coil has been created on the exterior and close to the yoke of each motor. The sensing coils have 50 turns and are connected to a large resistance 1 MΩ to emulate an open circuit. The stray rotating magnetic flux induces an electromotive force to the sensing coil, which is proportional to the penetrating magnetic flux. Such a sensor is illustrated later on for Motor C (Fig. 3).

TABLE I
CHARACTERISTICS OF THE THREE SIMULATED MOTORS

Characteristics	Motor A	Motor B	Motor C
Nominal Voltage	400 V	380 V	6.6 kV
Frequency	50Hz	60Hz	50Hz
Rated Power	4 kW	5.5 kW	1.1 MW
Number of poles	4	4	6
Stator slots	36	36	54
Rotor slots	28	44	70

A. FEA Results of Motors A and B

Both motor cases A and B have been simulated to operate under healthy and one broken rotor bar conditions at the same mechanical nominal load 26 Nm (100% rated load). The FE simulation calculated 4 seconds of steady state for each motor, while the speed ripple effect was taken into consideration.

The stray magnetic flux and the stator current have been extracted from the FEA with a sampling rate 10 kHz. Then the Fast Fourier Transform is calculated for all cases. The resulting spectra are illustrated in the following Fig. 1 and

Fig. 2 for Motor A and B respectively.

The appearance of the well-known $f_s \pm 2ksf_s$ fault related components (orange color arrows) are present in both the stray flux and stator current as expected in both motors suffering from a broken rotor bar. However, there is a distinct difference between the stray flux and the stator current. That is the appearance of the mechanical frequency related harmonics located at $f_s \pm f_r$ in the stray flux spectra, where $f_r = \frac{(1-s)}{p} f_s$ (black colour arrows). Those signatures appear to have by far the highest amplitudes among all fault related signatures. Furthermore, those harmonics are absent in the stator current. The mechanical frequency components have their own broken bar fault sidebands at frequencies $f_s \pm f_r \pm 2sf_s$ (blue colour arrows).
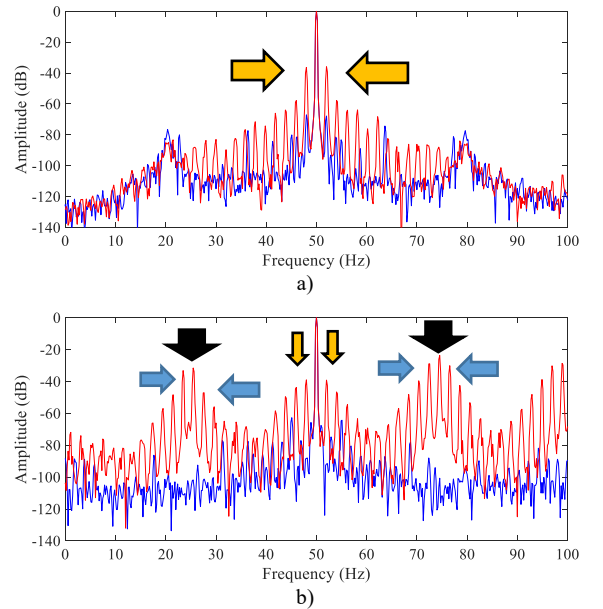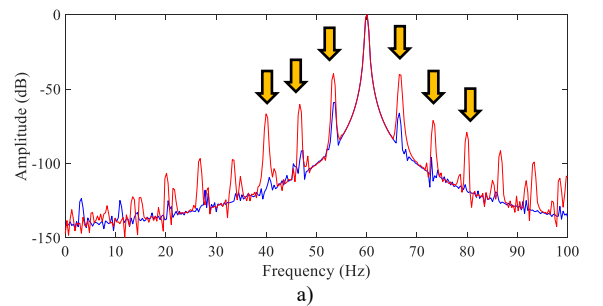

Fig. 1. Frequency spectra of: a) the stator current and b) the stray flux of the motor with 28 rotor bars under healthy (blue) and faulty (red) operation.
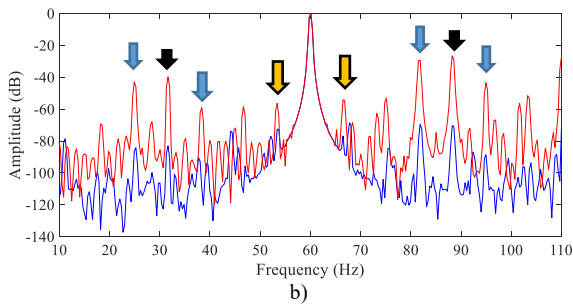

a)

Fig. 2. Frequency spectra of: a) the stator current and b) the stray flux of the motor with 44 rotor bars under healthy (blue) and faulty (red) operation.

The amplitudes of the fault related signatures because of the broken bar fault in the flux and current spectra are depicted in Tables II and III respectively.

Some remarks are the following regarding the stray flux results: It can be seen that, the right mechanical frequency sideband is less affected by the total number of rotor bars, while the amplitude difference between the two motors is only 3 dB. The same stands for its left broken rotor bar sideband, $f_s + f_r - 2sf_s$, which is practically the same between the two motors. The term "less affected" refers to the magnetic asymmetry caused by the fault. Both machines are 4-pole ones however the rotor bars per pole are different. For the Motor A it is 7, while for Motor B it is 11. In that sense, the fault severity of one broken bar and consequently the magnetic asymmetry caused by it is higher in Motor A.

TABLE II
SIGNATURE AMPLITUDES IN THE STRAY FLUX

Signature	Motor A	Motor B
fs-fr	-31.51 dB	-39.85 dB
fs+fr	-23.66 dB	-26.52 dB
fs-2sfs	-38.97 dB	-56.31 dB
fs+2sfs	-39.11 dB	-54.12 dB
fs-fr-2sfs	-33.16 dB	-42.86 dB
fs-fr+2sfs	-47.06 dB	-58.79 dB
fs+fr-2sfs	-28.95 dB	-29.42 dB
fs+fr+2sfs	-30.08 dB	-43.39 dB

TABLE III
SIGNATURE AMPLITUDES IN THE STATOR CURRENT

Signature	Motor A (healthy)	Motor A (faulty)	Motor B (healthy)	Motor B (faulty)
fs-4sfs	-81.25 dB	-57.77 dB	-91.49 dB	-60.26 dB
fs-2sfs	-67.04 dB	-36.31 dB	-59.04 dB	-39.55 dB
fs+2sfs	-67.76 dB	-35.87 dB	-66.08 dB	-40.14 dB
fs+4sfs	-81.4 dB	-57.71 dB	-95.75 dB	-71.03 dB

The reason behind the insensitivity of the right-hand side mechanical frequency harmonic and its associated broken bar sideband from the fault severity level is attributed to two factors. Firstly, those harmonics are produced by the speed ripple effect caused by torque pulsations. The torque pulsations are due to the $f_s - f_r$ component of the air-gap flux and the primary stator current of frequency f_s. That dependency associates the examined signatures with the combined moment of inertia of the rotor and load. Therefore, their amplitudes are affected less by the magnetic asymmetry caused by the broken bar. Secondly, the amplitude of the right mechanical frequency sideband is enhanced by the three times more frequency than the left one, as occurring from Faraday's law of induction.

The broken bar fault will induce the $f_s - f_r$ induced voltage to the sensor. As expected and seen from the results in Table II, this signature has stronger amplitude in Motor A. This happens because its cage has less bars and therefore one broken bar causes a greater magnetic asymmetry.

B. FEA Results of Motor C

Motor C has been simulated to operate under the nominal 11 kNm applied load torque (100% rated load). The speed ripple effect has been taken into consideration. The stray flux is captured with the application of a flux sensor placed on the stator's exterior. Part of the FEM Motor C model together with the flux sensor (pointed with a white arrow) is shown in Fig. 3 while the magnetic flux distribution is also illustrated under healthy operation. The flux sensor consists of a coreless coil with 50 turns and an in-series ohmic resistance 100 MΩ to account for the open circuit conditions.
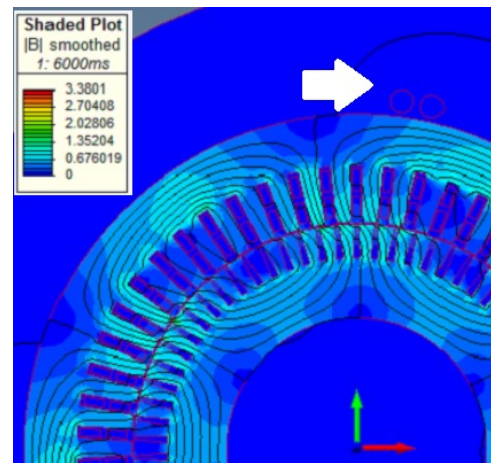

Fig. 3. Cross section of the 1.1MW induction motor FE model and magnetic flux spatial distribution in it.

The stator current and stray flux signals have been extracted and analyzed via the FFT. The resulting spectra are shown in Fig. 4. In all faulty cases, the mechanical frequency sidebands located at $f_s \pm kf_r$ appear with significant amplitudes in all cases. Those harmonics are absent in the healthy motor. Furthermore, the amplitudes of those signatures have a monotonic amplitude increase with the fault severity level. However, the broken rotor bar-related signatures are not visible. This happens because the speed of the motor is very close to the synchronous one (slip s<1%). This is usual in large electric motors. The low slip leads to broken bar sidebands, which are then hidden in the leakage

of the main harmonics such as the fundamental and the mechanical frequency ones. Despite that, the sensitivity of the mechanical frequency related sidebands on the fault severity level provides an obvious alarm for the fault existence, even at low slip operation.

This outcome is very satisfying for low slip operating motors. This is where the MCSA usually provides unreliable results. This is due to the inherent difficulty of monitoring of the broken rotor bar fault close to the fundamental stray flux harmonic. The amplitudes of the mechanical frequency components are shown in Table IV for all cases.

Signature	1 broken bar	2 broken bars	3 broken bars
fs-fr	-36.97 dB	-29.95 dB	-20.05 dB
fs+fr	-29.88 dB	-22.06 dB	-13.54 dB
fs-2fr	-46.51 dB	-39.46 dB	-29.36 dB
fs+2fr	-28.06 dB	-20 dB	-12.44 dB

C. Analysis of the Transient Behaviour via the Short Time Fourier Transform (STFT)

The analysis of machine signals during operation, using spectrograms is valuable because one can examine not only the harmonics' energy but also their frequency variations which are expressed as distinct trajectories. The stray flux has been used as a reliable diagnostic mean during the start-up of the induction motor [24]-[25]. The behavior is supposed to be similar to that of the stator current, where several fault components appear when there is a broken rotor bar fault, however the V-pattern of the $(1-2s)f_s$ is the most characteristic and distinct [26].

The motors are simulated to start from zero speed and accelerate up to the nominal load and steady state. The V-shape is clear in Motor C's stator current during the start-up under faulty operation, as shown in Fig. 5 (black arrows). Other fault related trajectories are also recognized such as the $(1-4s)f_s$ (purple arrow) and $(1+2s)f_s$ (blue arrow) harmonics. However, the fundamental harmonic sidebands are not distinctly clear in the stray flux in Fig. 6. On the other hand, a great number of additional harmonics' trajectories characterizes the stray flux spectra. Those trajectories are derived by the mechanical speed frequency sidebands around the stator time harmonics. Those harmonics create a net of trajectories in the start-up region of the induction motor which clearly reveals the fault however it is not easy to isolate each individual trajectory. At the steady state though, the trajectories are quite clear. The motors reach the steady state after approximately 1.5 s. The healthy motor's start-up is slightly longer than the faulty due to the increase of the rotor resistance due to the fault, which shifts the torque versus speed characteristic to the left leading to increase of the starting torque.
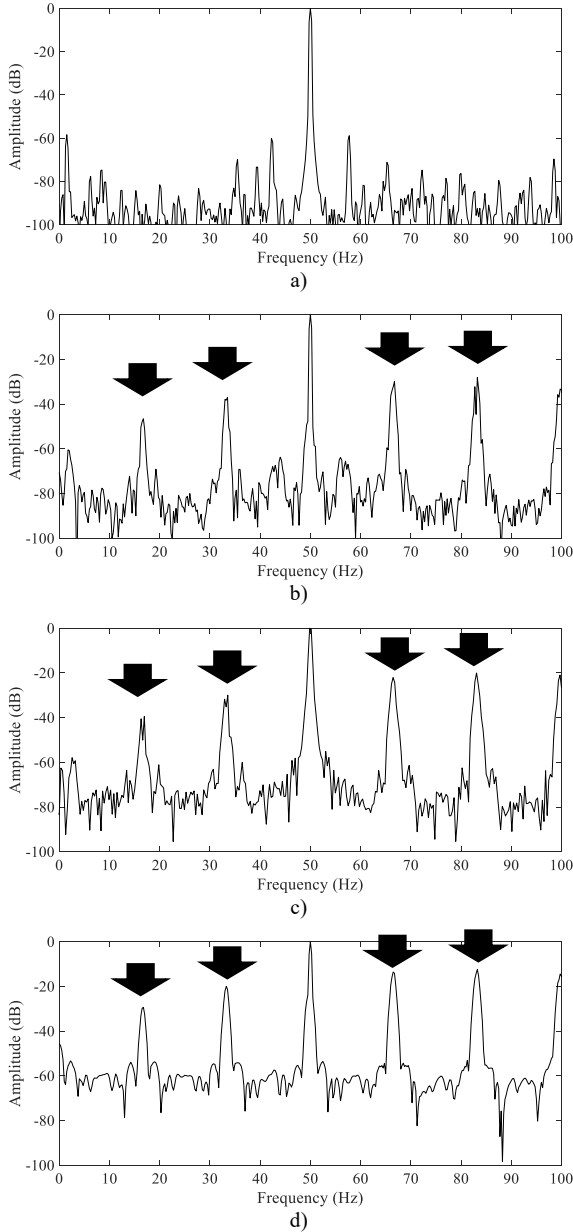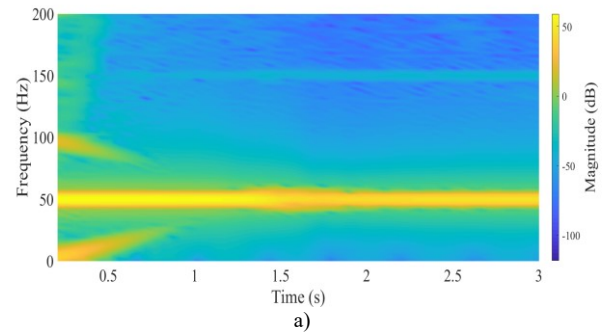

Fig. 4. Stray flux spectra of Motor C for: a) healthy operation, b) motor with 1broken bar, c) motor with 2 broken bars and d) motor with 3 broken bars.
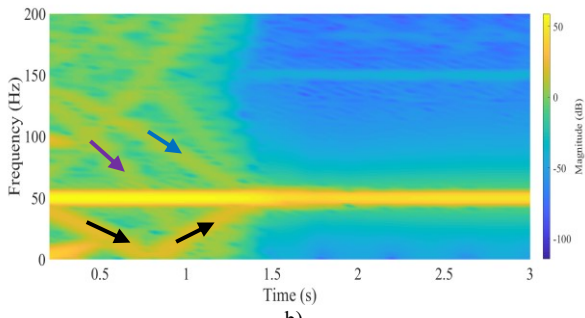

a)

b)

Fig. 5. The STFT spectrogram of the Motor C stator current under a) healthy operation and b) two adjacent broken rotor bars fault.
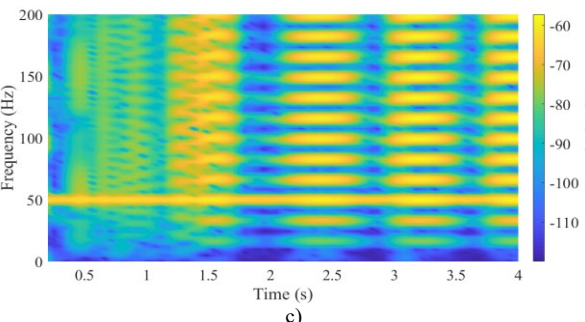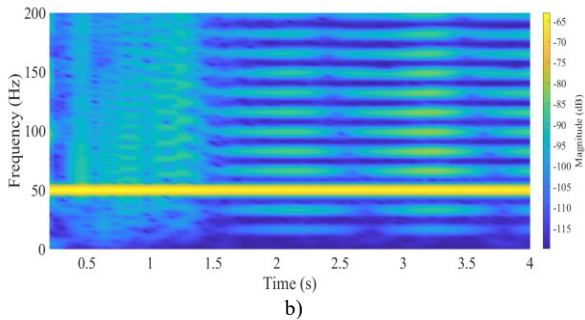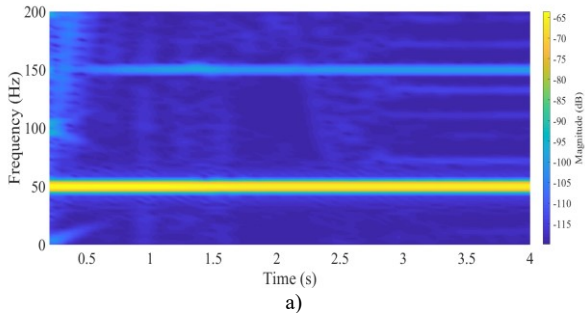

a)

b)

c)

Fig. 6. The STFT spectrogram of the Motor C stray flux under a) healthy operation b) one broken rotor bar and c) two adjacent broken rotor bars fault.

Similar spectra are calculated for Motor A, which has a fast transient, lasting approximately 0.3 seconds. The V-pattern is therefore not observable in the stator current (Fig. 7). For fast start-ups the stator current spectrogram looks similar between healthy and faulty conditions under the exception of the fault sidebands at higher frequencies. They are theoretically better visible with the increase of the load and therefore the slip. However, in this case the spectra look alike containing mainly the fundamental and third harmonics.

That is also the case for the stray flux shown in Fig. 8. The net of trajectories between stall and steady state are not observable due to the very fast transient. Despite that, at steady state, the whole family of mechanical frequency related harmonics $f_s \pm k(1-s)\frac{f_s}{p}$ is visible at frequencies that are submultiples of the supply one (approximately 25 Hz, 75 Hz, etc). Such trajectories can be used to differentiate the faulty from the healthy motor.
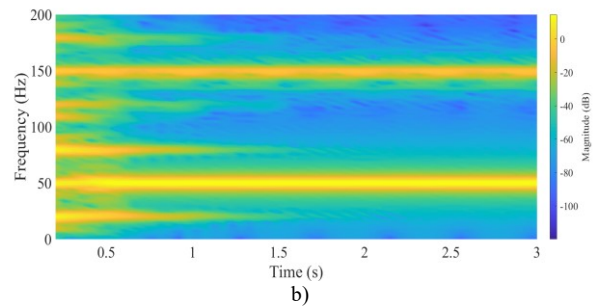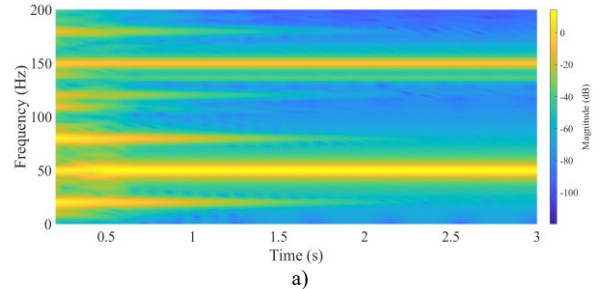

a)

b)

Fig. 7. The STFT spectrogram of the Motor A stator current under a) healthy operation and b) a broken rotor bar fault.
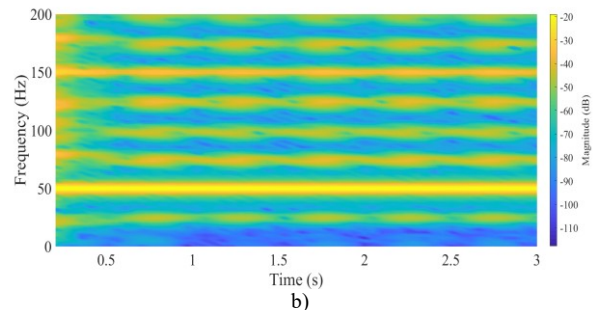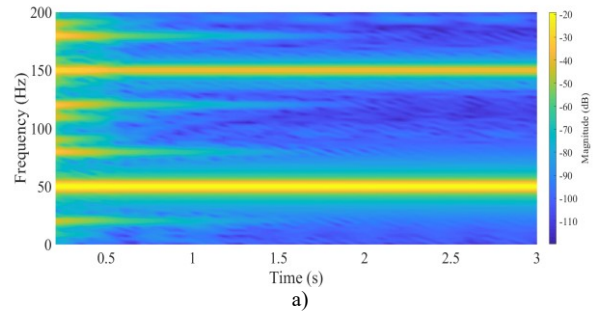

a)

b)

Fig. 8. The STFT spectrogram of the Motor A stray flux under a) healthy operation and b) a broken rotor bar fault.

III. EXPERIMENTAL TESTING

To test the validity of the FEA simulations, two identical squirrel-cage induction motors have been tested under healthy operation and under one broken rotor bar fault. The tested motors have the following characteristics: 400V, 50Hz, 4kW and 4 poles.

The experimental setup can be seen in the following Fig. 9. The induction motor has been mechanically coupled to a permanent magnet generator feeding a symmetrical 3-phase variable resistance. For safety purposes, the two machines are shielded in a protective Plexiglas box. A hole was drilled in one of the rotors in order to electrically disconnect one broken bar (Fig. 10). When the motor was disassembled, it was possible to determine the induction motor's slots, which are 36 and 32, for the stator and rotor respectively. Furthermore, the magnetic flux sensor positioned on the motor is shown in Fig. 11.
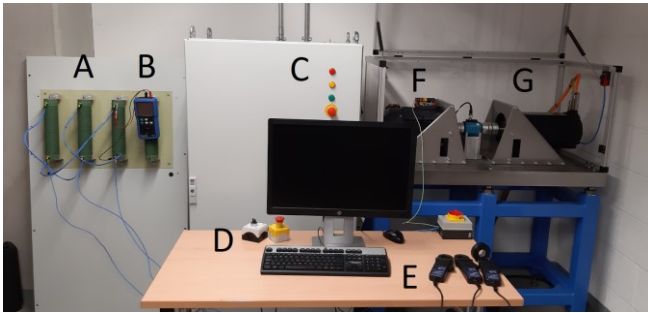

Fig. 9. The experimental test bed where: A) 3-phase ohmic resistance, B) digital voltage/current meter, C) power cabinet, D) protection switches, E) current clamps, F) induction motor and G) permanent magnet generator.

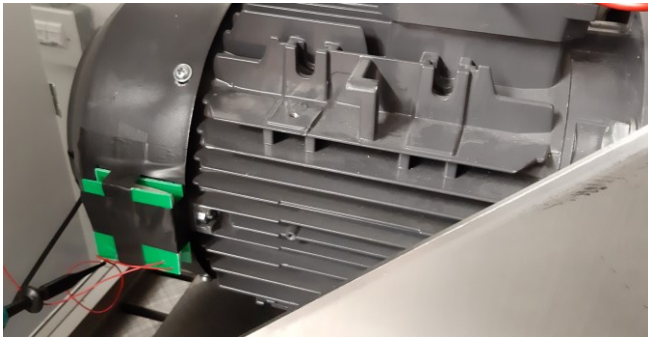Fig. 10. The rotor with one broken rotor bar.

Fig. 11. The magnetic flux sensor attached to the induction motor.

Using a commercial current probe, with a sensitivity of 10 mV/A and an accuracy of ±1% of reading at ±100/±500 mA, the stator currents of each motor were captured with a set of three identical current probes. Providing a safety BNC connector, this measurement was at later stage logged onto a digital high-resolution buffer memory unit used for acquisition of signal waveforms and data.

At the same time, the stray magnetic flux was captured with the use of an in-house built flux sensor (Appendix A), which was developed in the laboratory. The rigid search coil consists of 1500 turns wounded on a square-body reel of dimensions 40 x 40 mm for the main body and 55 x 55 mm for the salient edges at each top and bottom end of the reel. Additionally, the 8 mm slot height of the reel is full-filled with a 0.1 mm diameter distributed copper winding of resistance 3.4 Ω/m. For capturing the waveform of the voltage induced on the search coil, a voltage probe has been installed in order to clamp one of the two ending connectors of the sensor, while the other end of the sensor was grounded.

The multi-variable measurements of both the current and the stray flux signals were logged onto a high resolution, deep memory, 8-channel oscilloscope. Offering a 12-bit resolution and serial bus decoding with 256 MS buffer memory and a 20 MHz bandwidth, each signal waveform was captured within 12 frames of 10 sec each, providing the ability to gather extended waveforms over the steady state of the motors for reliable signal representation in both the time and frequency domain.

A. Monitoring at Steady State

Firstly, the motors have been set to operate at rated load conditions. More specifically, the supplied voltage is 400 V, the applied mechanical torque 26 Nm and the rotor speed is 1460 rpm. The comparative spectra of the stator current and stray flux are shown in the following Fig. 12 and 13 respectively. Moreover, the various signatures amplitudes are summarized in Table V. One first remark is that the inherent mixed eccentricity harmonic at f_s+f_r is totally absent in the stator current spectra of the healthy motor, while very weak in the faulty one. On the other hand, the same component is present in the stray flux for both cases. This is a clear indication that the mechanical frequency components in the stray flux are not necessarily eccentricity related. Moreover, they could be a useful indication of the rotor's inherent electrical imbalance due to porosity and magnetic anisotropy as well as load imbalance due to the hole that has been drilled to emulate the broken rotor bar fault. Moreover, the mixed eccentricity sideband at $f_s - f_r$ exists in both healthy and faulty induction motors. However its amplitude in the stator current is significantly lower than that of the stray flux. The rotor speed related components are marked with black arrows while the broken rotor bar ones with yellow.
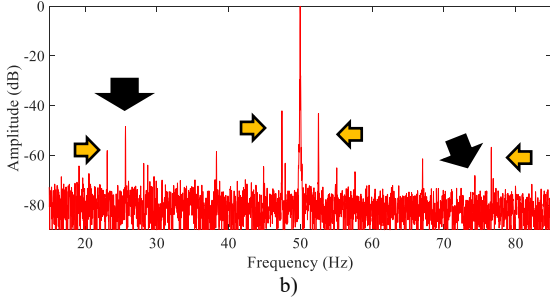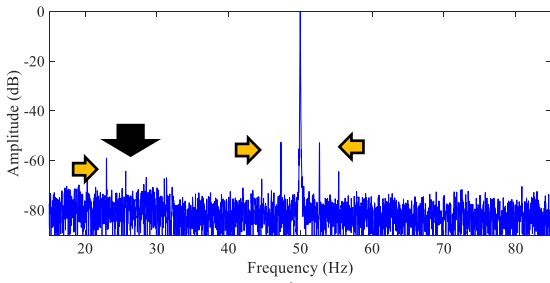
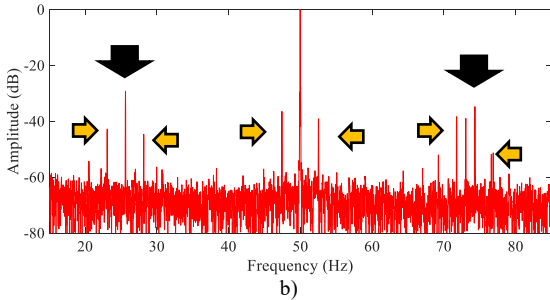Fig. 12. Stator current spectra for: a) healthy motor and b) motor with 1 broken rotor bar under rated load.

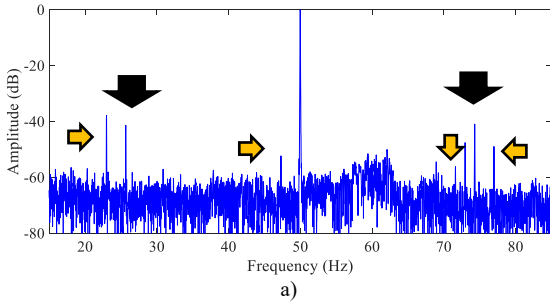
Fig. 13. Stray flux spectra for: a) healthy motor and b) motor with 1 broken rotor bar under rated load.

Furthermore, the fault signature at $f_s+f_r-2sf_s$ presents an impressive amplitude increase around 18 dB between the healthy and faulty cases. During the analysis with FEA, this signature appeared to have a certain immunity to the total number of rotor bars while its amplitude was greatly increased in the faulty motor case.

Additionally, the signature at $f_s - f_r + 2sf_s$ is absent in the healthy motor and has an impressive amplitude of -44.65 dB in the motor with the broken rotor bar. Finally, the traditional sidebands around the fundamental increase both as expected.

TABLE V
EXPERIMENTAL SIGNATURE AMPLITUDES IN THE STRAY FLUX

| Signature	Healthy	Faulty
fs-fr	-41.4 dB	-29.25 dB
fs+fr	-40.92 dB	-34.76 dB
fs-2sfs	-52.31 dB	-36.47 dB
fs+2sfs		-39.11 dB
fs-fr-2sfs	-37.82 dB	-42.79 dB
fs-fr+2sfs		-44.65 dB
fs+fr-2sfs	-56.16 dB	-38.37 dB
fs+fr+2sfs	-48.94 dB	-51.31 dB

IV. CONCLUSIONS

In this paper, the impact of the broken rotor bar fault on the mechanical frequency of the stray flux has been investigated with FEA and experimental testing. The results indicate that those signatures, which are known for eccentricity and load imbalances detection, increase with the broken rotor bar fault also. This finding sets a future challenge, which is the discrimination between rotor electrical and mechanical faults with the use of the stray flux. Furthermore, it appears that the mechanical frequency signatures offer satisfying broken bar diagnostic potential for large motors operating at very low slip where the traditional fault related signatures of both the flux and the stator current are masked from the leakage of the fundamental harmonics. The analysis of broken bar fault related sidebands around the mechanical frequency harmonics reveal also good diagnostic potential independently from the number of the rotor bars, which is not the case for the stator current primary sideband, the amplitude of which is directly dependent on the rotor cage bars number.

APPENDIX

The magnetic flux sensor geometry and dimensions are shown in the figure below:
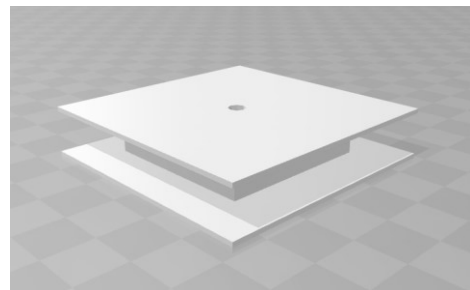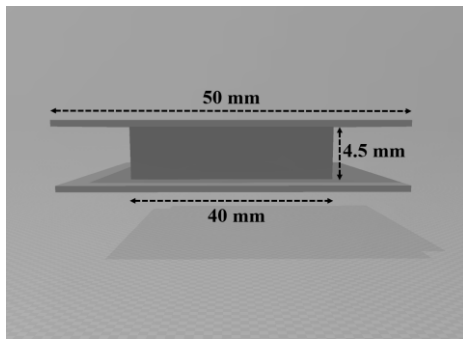
Top: 3D view of the designed coil reel
Bottom: the sensor body's side view with dimensions.

References

[1] A.Gandhi, T. Corrigan and L. Parsa, "Recent Advances in Modeling and Online Detection of Stator Interturn Faults in Electrical Motors", *IEEE Trans. Ind. Elec.*, Vol. 58, no. 5, pp. 1564-1575, 2011.

[2] P.J. Tavner, "Review of condition monitoring of rotating electrical machines", *IET Elec. Pow. Appl.*, Vol. 2, No. 4, pp. 215-247, 2008.

[3] A. A Salah, D. G. Dorrell and Y. Guo, "A Review of the Monitoring and Damping Unbalanced Magnetic Pull in Induction Machines Due to Rotor Eccentricity", *IEEE Trans. Ind. Appl.*, 2019, early access.

[4] H. Henao et al, "Trends in Fault Diagnosis for Electrical Machines: A Review of Diagnostic Techniques", *IEEE Ind. Elec. Mag.*, Vol. 8, No. 2, pp. 31-42, 2014.

[5] G.B. Kliman, R.A. Koegl,; J. Stein, R.D. Endicott and M.W. Madden, "Noninvasive detection of broken rotor bars in operating induction motors", *IEEE Trans. Ener. Conv.*, Vol. 3, No. 4, pp. 873-879, 1988.

[6] M. Drif and A. J. Marques Cardoso, "Discriminating the Simultaneous Occurrence of Three-Phase Induction Motor Rotor Faults and Mechanical Load Oscillations by the Instantaneous Active and Reactive Power Media Signature Analyses", *IEEE Trans. Ind. Elec.*, Vol. 59, No. 3, pp. 1630-1639, 2012.

[7] K. N. Gyftakis, D. V. Spyropoulos, J. C. Kappatou and E. D. Mitronikas, "A Novel Approach for Broken Bar Fault Diagnosis in Induction Motors Through Torque Monitoring", *IEEE Trans. Ener. Conv.*, Vol. 28, No. 2, pp. 267-277, 2013.

[8] K. N. Gyftakis, A. J. M. Cardoso and J. A. Antonino-Daviu, "Introducing the Filtered Park's and Filtered Extended Park's Vector Approach to Detect Broken Rotor Bars in Induction Motors Independently from the Rotor Slots Number", *Elsevier Mechanical Systems and Signal Processing*, Vol. 93, pp. 30-50, 2017.

[9] S. M. A. Cruz and A. J. M. Cardoso, "Stator winding fault diagnosis in three-phase synchronous and asynchronous motors by the extended Park's vector approach", *IEEE Trans. Ind. Appl.*, Vo. 37, No. 5, pp. 1227-1233, 2001.

[10] S. Shin, J. Kim, S.B. Lee, C. Lim, and E. J. Wiedenbrug, "Evaluation of the influence of rotor magnetic anisotropy on condition monitoring of 2 pole induction motors," *IEEE Trans. Ind. Appl.*, vol. 51, no. 4, pp. 2896-2904 , Sept 2014.

[11] P. A. Panagiotou, I. Arvanitakis, N. Lophitis , J. A. Antonino-Daviu and K. N. Gyftakis, "Analysis of Stray Flux Spectral Components in Induction Machines under Rotor Bar Breakages at Various Locations", ICEM 2018, Alexandroupoli, Greece, Sep. 2018.

[12] J. Antonino-Daviu, J. Pons-Llinares, S.B. Lee, "Advanced Rotor Fault Diagnosis for Medium-Voltage Induction Motors Via Continuous Transforms," *IEEE Trans. Ind. Appl.*, vol. 52, no. 5, pp. 4503-4509, Sept/Oct, 2016.

[13] J. Pons-Llinares, J. Antonino-Daviu, M. Riera-Guasp, S.B. Lee, T-J. Kang and C. Yang, "Advanced Induction Motor Rotor Fault Diagnosis Via Continuous and Discrete Time-Frequency Tools," *IEEE Trans. Ind. Elect.*, vol. 62, no. , pp. - , March, 2015.

[14] K. Abbaszadeh, J. Milimonfared, M. Haji M. and H. A. Toliyat, "Broken bar detection in induction motor via wavelet transformation", IEEE IECON, pp. 95-99, 2001.

[15] G. Didier, E. Ternisien, O. Caspary and H. Razik, "A new approach to detect broken rotor bars in induction machines by current spectrum analysis", *Elsevier Mech. Syst. Sign. Proc.*, Vol. 21, No. 2, pp. 1127-1142, 2007.

[16] D. Morinigo-Sotelo, R. J. Romero-Troncoso, P. A. Panagiotou, J. A. Antonino-Daviu and K. N. Gyftakis, "Reliable Detection of Broken Rotor Bars in Induction Motors via MUSIC and ZSC Methods", *IEEE Trans. Ind. Appl.*, Vol. 54, No. 2, pp. 1224 – 1234, 2018.

[17] A. Ceban, R. Pusca and R. Romary, "Study of Rotor Faults in Induction Motors using External Magnetic Field Analysis", *IEEE trans. Ind. Elec.*, Vol. 59, No. 5, pp. 2082-2093, 2012.

[18] L. Frosini, C. Harlisca and L. Szabo, "Induction Machine Bearing Fault Detection by Means of Statistical Processing of the Stray Flux Measurement", *IEEE Trans. Ind. Elec.*, Vol. 62, No. 3, pp. 1846-1854, 2015.

[19] G. Mirzaeva and K. I. Saad, "Advanced Diagnosis of Rotor Faults and Eccentricity in Induction Motors Based on Internal Flux Measurement", *IEEE Trans. Ind. Appl.*, Vol. 54, No. 3, pp. 2981-2991, 2018.

[20] G. Mirzaeva, K. I. Saad and M. G. Jahromi, "Comprehensive Diagnostics of Induction Motor Faults Based on Measurement of Space and Time Dependencies of Air Gap Flux", *IEEE Trans. Ind. Appl.*, Vol. 53, No. 3, pp. 2657-2666, 2017.

[21] G. M. Joksimović, J. Riger, T. M. Wolbank, N. Perić and M. Vašak, "Stator-Current Spectrum Signature of Healthy Cage Rotor Induction Machines", *IEEE Trans. Ind. Elec.*, Vol. 60, No. 9, pp. 4025-4033, 2013.

[22] Y. Park, C. Yang, J. Kim, H. Kim, S.B. Lee, K.N. Gyftakis, P. Panagiotou, S.H. Kia and G. Capolino, "Stray Flux Monitoring for Reliable Detection of Rotor Faults under the Influence of Rotor Axial Air Ducts ," *IEEE Trans. Ind. Electr.*, Vol. 66, No. 10, pp. 7561-7570, 2019.

[23] K. N. Gyftakis, P. A. Panagiotou and S. B. Lee, "The Role of the Mechanical Speed Frequency on the Induction Motor Fault Detection via the Stray Flux", IEEE SDEMPED 2019, Toulouse, France, 2019.

[24] J. A. Ramirez-Nunez, J. A. Antonino-Daviu, V. Climente-Alarcón, A. Quijano-López, H. Razik, R. A. Osornio-Rios and R. de J. Romero-Troncoso, "Evaluation of the Detectability of Electromechanical Faults in Induction Motors Via Transient Analysis of the Stray Flux", *IEEE Trans. Ind. Appl.*, Vol. 54, No. 5, pp. 4324-4332, 2018.

[25] M. E. Iglesias-Martínez, P. Fernández de Córdoba, J. A. Antonino-Daviu and J. Alberto Conejero, "Detection of Nonadjacent Rotor Faults in Induction Motors via Spectral Subtraction and Autocorrelation of Stray Flux Signals", *IEEE Trans. Ind. Appl.*, Vol. 55, No. 5, pp. 4585-4594, 2019.

[26] C. Yang, T.-J. Kang, D. Hyun, S. B. Lee, Jose A. Antonino-Daviu and J. Pons-Llinares, "Reliable Detection of Induction Motor Rotor Faults Under the Rotor Axial Air Duct Influence", *IEEE Trans. Ind. Appl.*, Vol. 50, No. 4, pp. 2493-2502, 2014.

AUTHORS' INFORMATION

Konstantinos N. Gyftakis (M'11, SM'20) was born in Patras, Greece, in May 1984. He received the Diploma in Electrical and Computer Engineering from the University of Patras, Greece in 2010. He pursued a Ph.D in the same institution in the area of electrical machines condition monitoring and fault diagnosis (2010-2014). Then he worked as a Post-Doctoral Research Assistant in the Dept. of Engineering Science, University of Oxford, UK (2014-2015). Between 2015-2018 and 2018-2019 he was a Lecturer and a Senior Lecturer respectively, on Electrical and Electronic Engineering, School of Computing, Electronics and Mathematics and an Associate with the Research Institute for Future Transport and Cities, Coventry University, UK.

Since 2019, he has been a Lecturer in Electrical Machines in the University of Edinburgh, UK and a Member of the Institute for Energy Systems. the same institution. Additionally, since 2016 he has been a member of the "Centro de Investigação em Sistemas Electromecatrónicos" (CISE), Portugal.

He has authored/co-authored more than 90 papers in international scientific journals and conferences and a chapter for the book: "Diagnosis and Fault Tolerance of Electrical Machines, Power Electronics and Drives", IET, 2018. He is an IEEE Senior Member, as well as member of the IEEE IAS and IEEE IES.
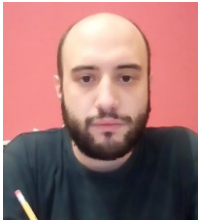
Panagiotis A. Panagiotou was born in Thessaloniki, Greece, in 1989. He received the 5 year Diploma in Electrical & Computer Engineering from the University of Patras, Greece, in 2015 and the MSc in Complex Systems & Network Theory from Aristotle University of Thessaloniki, Department of Mathematics in 2016. Currently, he is a Ph.D Candidate at Coventry University, UK.

His research is focused on condition monitoring and fault diagnosis of electric motors for industrial and EV applications, as well as statistical modelling and signal processing for diagnostic purposes.

Sang Bin Lee (S'95–M'01–SM'07–F'17) received the B.S. and M.S. degrees from Korea University, Seoul, Korea, in 1995 and 1997, respectively, and the Ph.D. degree from the Georgia Institute of Technology, Atlanta, GA, USA, in 2001, all in electrical engineering.

From 2001 to 2004, he was with the General Electric Global Research Center, Schenectady, NY, USA, where he worked on development of test methods for generators and motors. From 2010 to 2011, he was with the Austrian Institute of Technology, Vienna, Austria, where he worked on condition monitoring of permanent magnet synchronous machines. From 2017 to 2018, he was a Consultant at Qualitrol - Iris Power Engineering, Toronto, and a Visiting Researcher at University of Waterloo, ON, Canada, where he worked on testing of medium-high voltage machines. Since 2004, he has been a Professor of Electrical Engineering with Korea University. His research interests include testing, condition monitoring, and diagnostics of electric machines and drives.

Dr. Lee was the recipient of the 2017 Diagnostics Achievement Award from IEEE Symposium on Diagnostics of Electric Machines Power Electronics and Drives (SDEMPED) Conference. He received fourteen Prize Paper Awards from the IEEE Industry Applications Society (IAS), IEEE Power Engineering Society, Electric Machines, Industrial Drives, and Pulp and Paper Industry Committees of the IEEE IAS, Technical Committee on Diagnostics of the IEEE Power Electronics Society, and IEEE SDEMPED. He served a 2014–2016 Distinguished/Prominent Lecturer for the IEEE IAS, and an Associate Editor of the IEEE TRANSACTIONS ON INDUSTRY APPLICATIONS for the IEEE IAS Electric Machines Committee.